ELSEVIER

Volume 182, Number 6, June 2009

JOURNAL OF SOLID STATE CHEMISTRY

www.elsevier.com/locate/jssc

CONTENTS

Abstracted/indexed in BioEngineering Abstracts, Chemical Abstracts, Coal Abstracts, Current Contents/Physics, Chemical, & Earth Sciences, Engineering Index, Research Alert, SCISEARCH, Science Abstracts, and Science Citation Index. Also covered in the abstract and citation database SCOPUS®. Full text available on ScienceDirect®.

Regular Articles

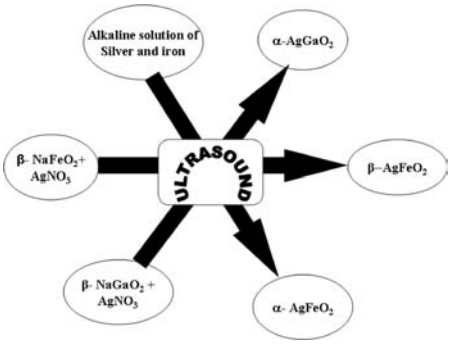

The application of ultrasound in the formation of α and β-forms of $AgMO_2$ (M = Fe, Ga) has been demonstrated.

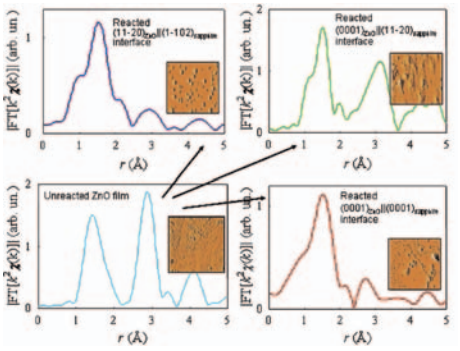

EXAFS Fourier transforms and morphology of different reactive interfaces between ZnO and Al_2O_3.

Regular Articles—Continued

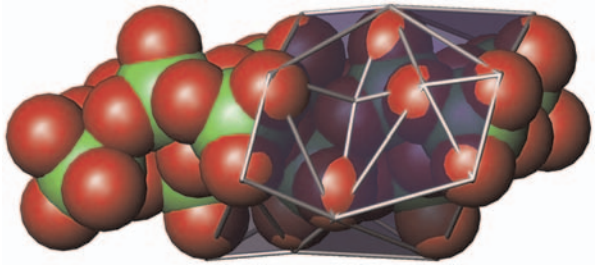

A geometric decomposition method for surface area determination is presented in the context of charge density matching in new organically templated polyoxomolybdates.

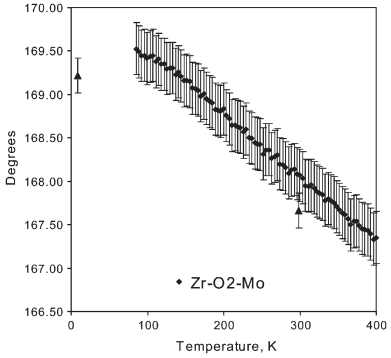

Negative thermal expansion in $Zr_2(MoO_4)(PO_4)_2$ is associated with a complex pattern of structural changes that is not the same as that previously reported for $Sc_2(WO_4)_3$.

Continued

Structure and crystal chemistry of fluorite-related $Bi_{38}Mo_7O_{78}$ from single crystal X-ray diffraction and *ab initio* calculations
Neeraj Sharma, René B. Macquart, Mogens Christensen, Maxim Avdeev, Yu-Sheng Chen and Chris D. Ling
Page 1312

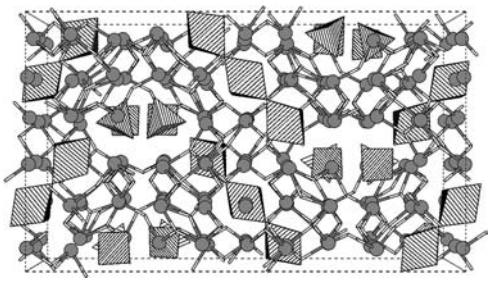

The crystal structure of $Bi_{38}Mo_7O_{78}$ with MoO_4 and MoO_6 represented as polyhedra, Bi atoms as gray spheres, and fluorite-type O atoms as white vertices of Bi–O–Bi bonds.

Magnetic and structural properties of Na*Ln*$MnWO_6$ and Na*Ln*$MgWO_6$ perovskites
Graham King, Lora M. Wayman and Patrick M. Woodward
Page 1319

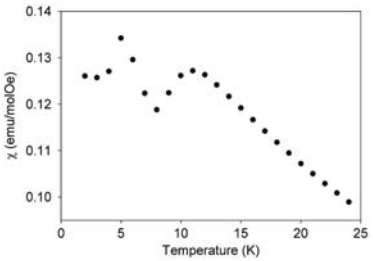

Evidence for multiple magnetic phase transitions in the *A* and *B*-site ordered perovskite $NaPrMnWO_6$.

Phase transformation of boron nitride under hypothermal conditions
Gang Lian, Xiao Zhang, Lingling Zhu, Deliang Cui, Qilong Wang and Xutang Tao
Page 1326

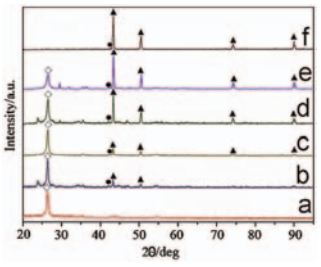

Phase transformations from hBN to wBN and cBN happened with the temperature increasing from 230 to 300 °C under hypothermal conditions, and nearly pure cBN has been synthesized at 300 °C and 12 MPa.

Reinvestigation and superstructure of $La_{3.67}[Fe(C_2)_3]$
Bambar Davaasuren, Enkhtsetseg Dashjav, Guido Kreiner, Horst Borrmann and Rüdiger Kniep
Page 1331

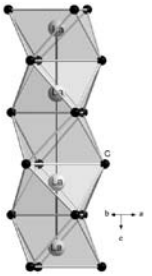

Diffraction data reveal a superstructure with weak superstructure reflections for $La_{3.67}[Fe(C_2)_3]$ in the space group $P6_3/m$. The superstructure is caused by an ordered arrangement of La atoms along 0, 0, *z* with alternating short and long distances.

Kinetics of Mn_2O_3 digestion in H_2SO_4 solutions
Daud K. Walanda, Geoffrey A. Lawrance and Scott W. Donne
Page 1336

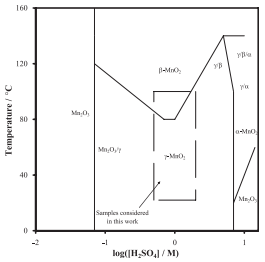

Manganese dioxide phase diagram resulting from the acid digestion of Mn_2O_3.

The $A^{2+}Mn_5(SO_4)_6$ family of triangular lattice, ferrimagnetic sulfates
D.V. West, T.M. McQueen, I.D. Posen, X. Ke, Q. Huang, H.W. Zandbergen, A.J. Williams, P. Schiffer and R.J. Cava
Page 1343

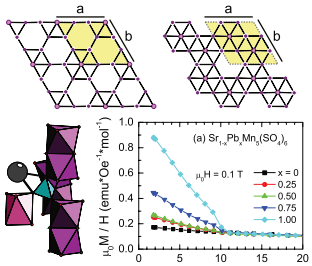

A new family sulfates, $A^{2+}Mn_5(SO_4)_6$ (A = Pb, Ba, Sr) is reported. Structures are solved by powder neutron diffraction. $PbMn_5(SO_4)_6$ is trigonal with lattice parameters of $a = 14.551(1)$ Å and $c = 7.535(1)$ Å. The structure has dimers of face-sharing MnO_6 octahedra, and two complementary triangular layers of Mn atoms that result in a ferrimagnet. All compounds magnetically order at 10 K. Low field susceptibility varies systematically with non-magnetic cation radius.

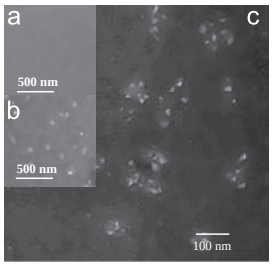

HRSEM micrograph of acid etched surface of silver doped sodium and niobium phosphate glass after nucleation heat treatment before (a) and after second heat treatment (b), (c) leading to phase separation and crystallization.

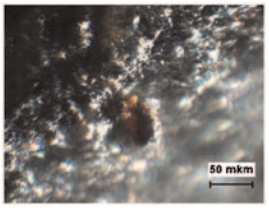

Chemical interaction and phase transformations in the B–BN system have been *in situ* studied by X-ray diffraction with synchrotron radiation at pressures up to 5.3 GPa and temperatures up to 2800 K using multianvil press. Three boron subnitrides have been synthesized and characterized.

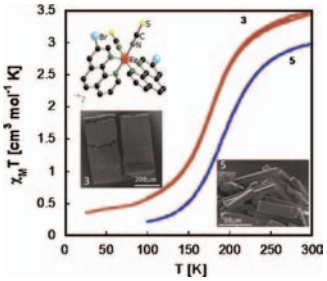

New Fe^{II} complexes of formula $[Fe(3\text{-Br-phen})_2(NCS)_2]$…Solvent have been synthesized by precipitation (**1**) and extraction (**4**) methods. ^{57}Fe Mössbauer and magnetic investigation reveal unique features atypical of classic $[Fe(phen)_2(NCS)_2]$ polymorphs. Complex **1**, undergoes upon cooling below room temperature an incomplete and gradual thermally induced spin conversion, while **4** remains mostly in the low-spin state. Role of supramolecular interactions, particles size, lattice solvents have profound influence on magnetic properties.

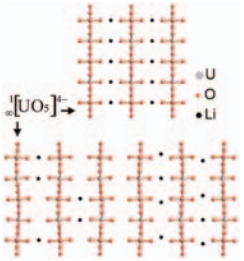

The three new lithium uranyl phosphates $Li_2(UO_2)_3(PO_4)_2O$, $Li(UO_2)_4(PO_4)_3$ and $Li_3(UO_2)_7(PO_4)_5O$ were synthesised via solid state reaction. The structures of these compounds are based upon three-dimensional open-frameworks built from $^1_\infty[UO_5]^{4-}$ chains connected through two types of layers, S and D, in the sequences S–S, D–D and S–D, respectively. The lithium atoms distribution along the channels induces various distortions of the $^1_\infty[UO_5]^{4-}$ chains.

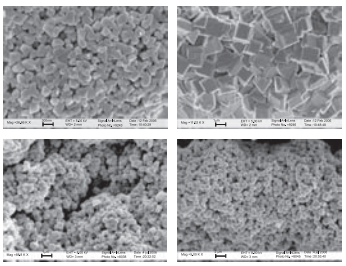

Novel MnO nano- and microparticles were controlled synthesized by solid-state thermolysis of inorganic core containing molecular clusters $[Mn_{12}O_{12}(O_2CR)_{16}(H_2O)_4]$ ($R = C_6H_5$, CH_3, and $C_6H_5OCH_2$) in a conventional tubular furnace.

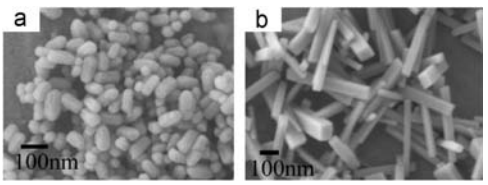

Hexagonal phase $BiPO_4$ nano-cocoons were fabricated by solvothermal method at 200 °C for 1 h. When the reaction time was increased to 3 h, monoclinic phase $BiPO_4$ nanorods were formed.

Continued

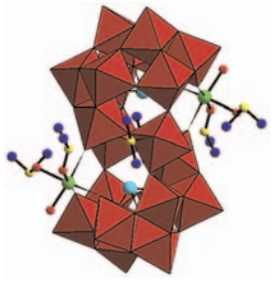

The first Ru^{III}-supported tungstoantimonate $[Ru^{II}(bpy)_3]_2[Sb_2W_{20}Ru_2^{III}(H_2O)_2(dmso)_6O_{68}]\cdot 3dmso$ (bpy = bi-pyridine) (**1a**) has been synthesized using $Ru(bpy)_3Cl_2$ as an alternative ruthenium-source and structurally characterized.

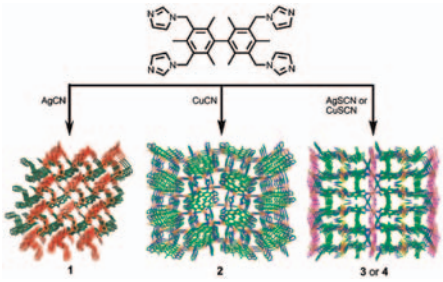

Four coordination polymers built upon Ag(I)/Cu(I) pseudohalides and a imidazolate ligand have been solvothermally synthesized. The luminescent properties for these compounds and the possible ferroelectric behavior of **1** are discussed.

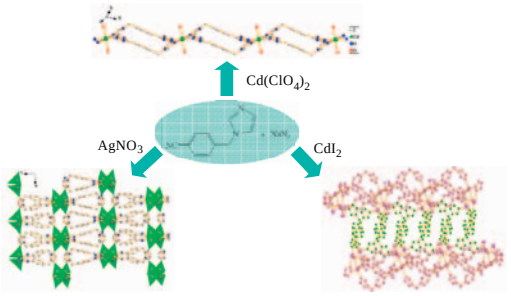

Three novel coordination polymers were obtained with in situ ligand formation through Sharpless's [3 + 2] reaction. The structure and luminescence properties of the complexes were investigated.

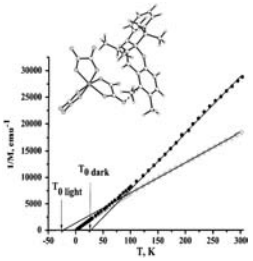

Fragment of crystal structure of $(Sp_3Cr(C_2O_4)_3)$. Temperature dependences of reciprocal molar magnetic moment of the sample at $T = 2$ K: (1) before irradiation, and (2) after UV irradiation.

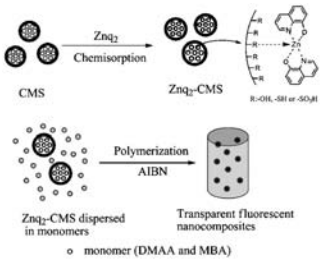

Znq_2–functionalized colloidal mesoporous silicas (Znq_2–CMS)/polymer transparent fluorescent nanocomposites were prepared by in situ bulk polymerization. The figure shows the synthetic scheme for the Znq_2–CMS and their transparent bulk nanocomposites.

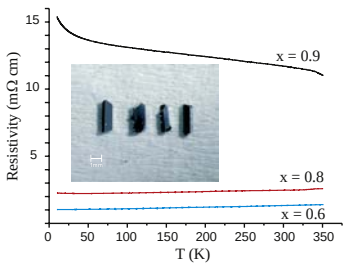

Alloys of the sphalerite-type solid solution $[ZnSnSb_2]_{1-x}[2(InSb)]_x$ can be prepared over the whole range of composition by Sn flux synthesis. A metal–nonmetal transition takes place between the compositions $x = 0.8$ and $x = 0.9$.

Syntheses, crystal structures and fluorescent properties of Cd(II), Hg(II) and Ag(I) coordination polymers constructed from 1H-1,2,4-triazole-1-acetic acid

De-Gang Ding, Li-Xia Xie, Yao-Ting Fan, Hong-Wei Hou and Yan Xu

Page 1443

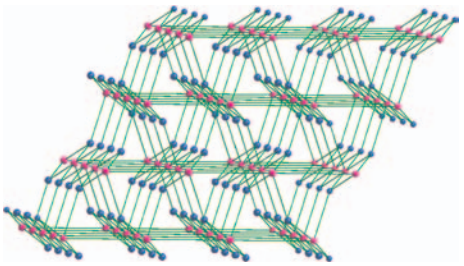

Three new compounds based on 1H-1,2,4-triazole-1-acetic acid and Cd(II), Hg(II) and Ag(I) salts display luminescent properties and may be potential candidates for luminescent materials.

Synthesis and characterization of quaternary chalcogenides $InSn_2Bi_3Se_8$ and $In_{0.2}Sn_6Bi_{1.8}Se_9$

Ming-Fang Wang, Shyue-Ming Jang, Jih-Chen Huang and Chi-Shen Lee

Page 1450

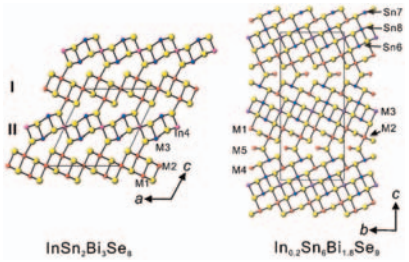

Quaternary selenides $InSn_2Bi_3Se_8$ and $In_{0.2}Sn_6Bi_{1.8}Se_9$ feature three-dimensional frameworks containing NaCl-(311) type slabs with varied thicknesses. Measurements of the electrical conductivity indicate that these materials are *n*-type semiconductors.

Syntheses and structures of three *f*-element selenite/hydroselenite compounds

Wendy L. Burns and James A. Ibers

Page 1457

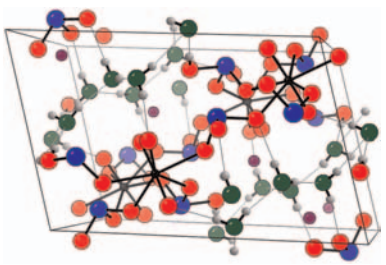

Structure of $Ce[U(SeO_3)(HSeO_3)] \cdot 3H_2O$ (Cs, purple; U, black; Se, blue; O, red; O_w, green; H, gray).

Dispersion control and nematic ordering of Ni/Al layered double hydroxide suspensions

Lingyu Luan, Shangying Liu and Dejun Sun

Page 1462

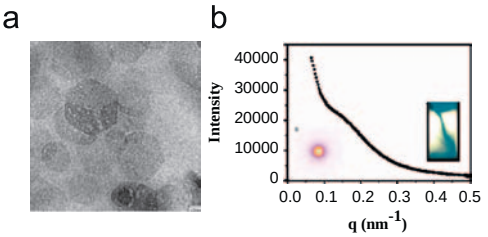

Well-defined Ni/Al LDH nanoparticles were prepared and nematic ordering confirmed by birefringence observations and SAXS measurements is observed in concentrated Ni/Al LDH suspensions.

Low-temperature heat capacity of triangle antiferromagnetic molecular clusters $K_{12}[(VO)_3(SbW_9O_{33})_2] \cdot 15H_2O$ and $K_{12}[(VO)_3(BiW_9O_{33})_2] \cdot 29H_2O$

Yoshimitsu Kohama, Hitoshi Kawaji, Tooru Atake, Keisuke Fukaya and Toshihiro Yamase

Page 1468

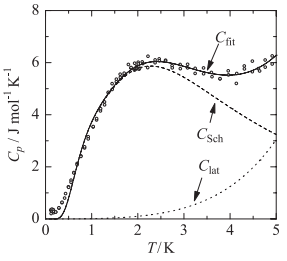

Temperature dependence of heat capacity for $K_{12}[(VO)_3(SbW_9O_{33})_2] \cdot 15H_2O$ below 5 K. This is well described by the model with a doublet ground state.

Nickel deficiency in $RENi_{2-x}P_2$ (RE = La, Ce, Pr). Combined crystallographic and physical property studies

Svilen Bobev, Sheng-qing Xia, Eric D. Bauer, Filip Ronning, Joe D. Thompson and John L. Sarrao

Page 1473

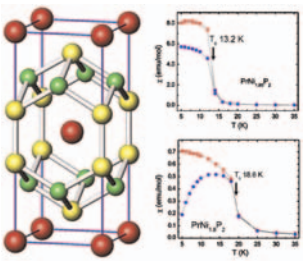

The non-stoichiometric $RENi_{2-x}P_2$ phases (RE = La, Ce, Pr), whose average structure belongs to the $ThCr_2Si_2$ type, are shown to exist with a wide range of defects on the transition metal site. The changes in the Ni-underoccupancy affect the magnetism of the synthesized materials.

Continued

Ionic diffusion mastering using crystal-chemistry parameters: τ-$Cu_{1/2}Ag_{1/2}V_2O_5$ structure determination and comparison with refined δ-$Ag_xV_2O_5$ and ε-$Cu_xV_2O_5$ ones
P. Rozier, M. Dollé and J. Galy
Page 1481

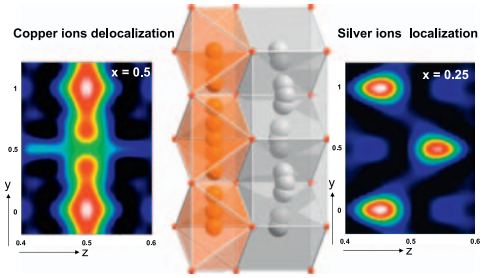

The role of nature and amount of guest species on their respective localisation Evidence for full delocalisation of copper ions and diffusion pathways visualisation.

B-site disordering in $Ba_3Ln_2MoO_9$ (Ln = Ho, Er) perovskites: A neutron diffraction study
S.A. Larrégola, J.A. Alonso, M. García Hernandez, M.T. Fernandez-Díaz and J.C. Pedregosa
Page 1492

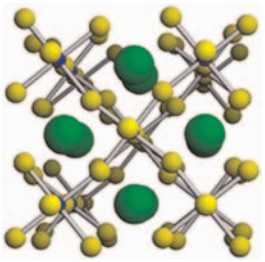

Preparation, structure and magnetic properties of $Ba_3Ln_2MoO_9$ ($Ln = Ho^{3+}$ and Er^{3+}) are descripted. Joint XRPD and NPD refinements confirm a tetragonal I4/*mcm* structure. *Ln* and Mo atoms are found to be distributed at random over the octahedral sites of the perovskites.

Solvothermal syntheses and structures of indium(III)-binaphthalenyl dicarboxylate complexes with yellow/blue luminescence
Qiang Gao, Fei-Long Jiang, Ming-Yan Wu, You-Gui Huang, Lian Chen, Wei Wei and Mao-Chun Hong
Page 1499

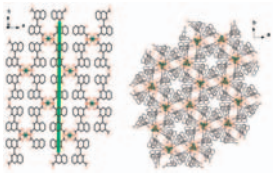

Two indium(III)-bna compounds were solvothermally synthesized. **1** adopts an unprecedented 2D chiral layer. **2** is constructed by –In–O–In– chains, which are further connected by bna^{2-} into a 3D honeycomb framework.

$Cr_xRe_{1-x}O_2$ oxides with different rutile-like structures: changes in the electronic configuration and resulting physical properties
D. Mikhailova, H. Ehrenberg, D. Trots, G. Brey, S. Oswald and H. Fuess
Page 1506

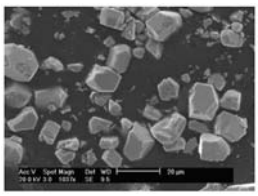

Antiferromagnetic rhenium oxides $Cr_xRe_{1-x}O_2$ with metallic type of conductivity crystallize in different rutile-like polymorphs depending on synthesis conditions. Single crystals of the tetragonal modification can be obtained by high-pressure high-temperature synthesis.

High-temperature structural phase transition in $Ca_2Fe_2O_5$ studied by *in-situ* X-ray diffraction and transmission electron microscopy
Hannes Krüger, Volker Kahlenberg, Václav Petříček, Fritz Phillipp and Waltraud Wertl
Page 1515

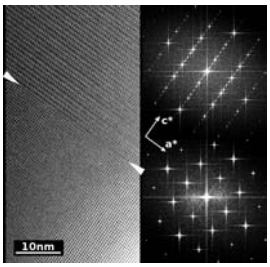

High-temperature HRTEM (zone axis [010]) of a phase boundary between domains of the *Pnma* (lower left) and *Imma(00g)s00* (upper right) structure. Micrograph recorded at 970 K. Corresponding FFT patterns are shown on the right.

Structural and electrical properties evolution in $Ba_{1-x}Sr_xRuO_3$ synthesized under high pressure
Jinggeng Zhao, Liuxiang Yang, Yong Yu, Fengying Li, Richeng Yu and Changqing Jin
Page 1524

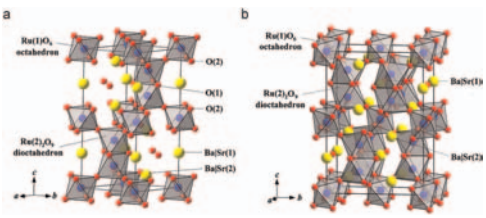

The 6H ($x \leqslant 0.3$) and 6M ($0.4 \leqslant x \leqslant 0.6$) $Ba_{1-x}Sr_xRuO_3$ solutions synthesized under high pressure adopt the normal and distorted hexagonal $BaTiO_3$ structures, respectively.

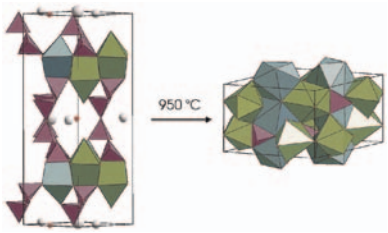

By heating over 900 °C Tb/Na tobermorite a terbium silicate apatite was obtained. The same product has been independently prepared and structurally characterized from powder diffraction data. Attempts of crystallizing terbium silicate apatite from melted NaF led to Tb_4O_7 crystals.

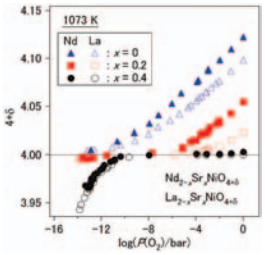

We synthesized $Nd_{2-x}Sr_xNiO_{4+\delta}$ by citric acid method and measured oxygen nonstoichiometry in the temperature range between 873 and 1173 K. They showed both oxygen excess and oxygen deficient composition depending on $P(O_2)$, temperature, and. the Sr content. The results are compared with the oxygen nonstoichiometry of $La_{2-x}Sr_xNiO_{4+\delta}$.

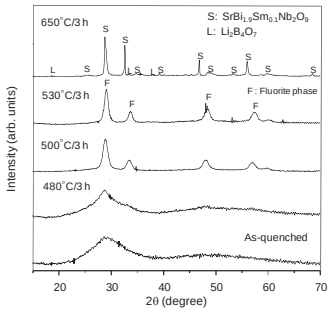

This figure shows the XRD patterns at room temperature for the as-quenched and heat treated samples in Sm_2O_3-doped ($x = 0.1$) glass. Based on these results, it is concluded that the formation of samarium-doped perovskite SBN phase takes place via an intermediate fluorite-like phase in the crystallization of this glass.

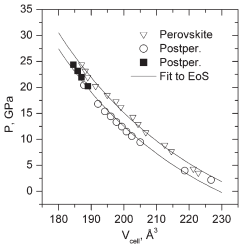

Fit of P–V data obtained from high-pressure X-ray diffraction study of perovskite and postperovskite $NaZnF_3$ to the third-order Birch–Murnaghan equation of state (solid line). Open and closed symbols represent experimental data corresponding to compression and decompression, respectively. Bulk moduli, $K_{0,P}$, of perovskite and postperovskite phases are 64.98 ± 2.67 and 69.88 ± 3.69 GPa.

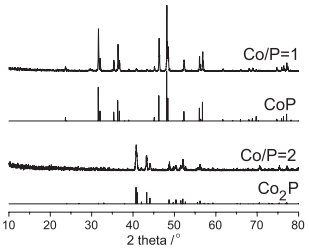

Metal phosphides were obtained stoichiometrically from their oxidic precursors by hydrogen plasma reaction under mild conditions.

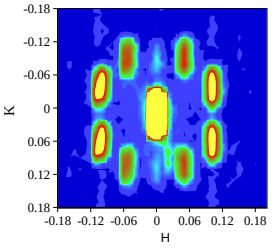

Ga_2Te_3 crystallizes into the zinc-blende structure, where one third of the cation sites are vacant. Single crystal X-ray diffraction studies showed that as-grown Ga_2Te_3 crystals display main reflections which correspond to the cubic zinc-blende lattice and satellite reflections at $q = (0.089\,0.050\,0.00)_c$. These satellite reflections show that Ga_2Te_3 crystals contain transverse type displacement modulation, whose traveling direction is almost $\langle 210 \rangle_c$, while the polarization vector is nearly $\langle 001 \rangle_c$.

Continued

Influence of fuel-to-oxidizer ratio on the magnetic properties of Fe-doped In_2O_3 nanoparticles synthesized by solution combustion method

J. Yu, L.B. Duan, Y.C. Wang and G.H. Rao

Page 1563

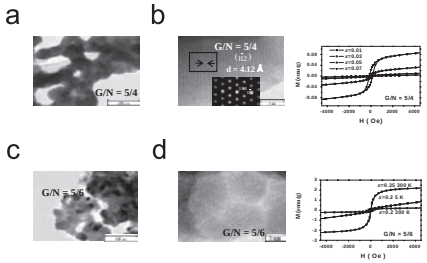

The G/N ratio (5/4 and 5/6, respectively) has a prominent effect on the particle size and magnetic properties of Fe-doped In_2O_3 nanoparticles.

Twinned crystal structure and compressibility of $TlTeVO_5$

Andrzej Grzechnik, P. Shiv Halasyamani, Hong Young Chang and Karen Friese

Page 1570

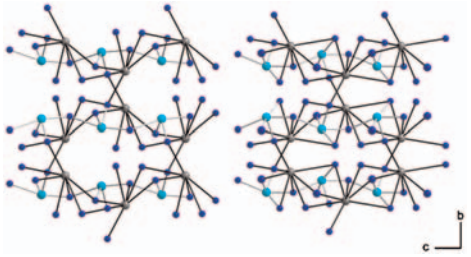

Coordination spheres of the Tl and Te atoms at ambient pressure (left) and at 7.11 GPa (right). The medium gray, cyan, and blue symbols are the Tl, Te, and O atoms, respectively. The Tl–O and Te–O distances below 3.5 and 2.5 Å are drawn, respectively.

Preparation of gold microparticles using halide ions in bulk block copolymer phases via photoreduction

Sang-Ho Cha, Ki-Hyun Kim, Won-Ki Lee and Jong-Chan Lee

Page 1575

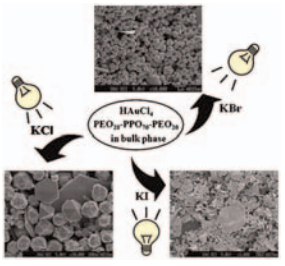

Gold microparticles were successfully prepared using halide ions as additives in the polymeric bulk phase via photoreduction with the glow lamp irradiation.

Synthesis of anatase nanoparticles with extremely wide solid solution range and $ScTiNbO_6$ with α-PbO_2 structure

Masanori Hirano and Takaharu Ito

Page 1581

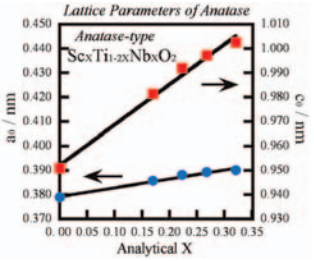

Anatase-type $Sc_XTi_{1-2X}Nb_XO_2$ solid solutions with wide solid solution range ($X = 0$–0.35) were hydrothermally formed as nanoparticles from the precursor solutions of $Sc(NO_3)_3$, $TiOSO_4$, $NbCl_5$ at 180 °C for 5 h using the hydrolysis of urea. Anatase-type $ScTiNbO_6$ was synthesized under hydrothermal condition. $ScTiNbO_6$ having α-PbO_2 structure with possibly some cation order similar to that seen in wolframite was formed through phase transformation above 900 °C.

Synthesis, characterization and formation process of transition metal oxide nanotubes using carbon nanofibers as templates

Hitoshi Ogihara, Sadakane Masahiro, Yoshinobu Nodasaka and Wataru Ueda

Page 1587

Mono and binary transition metal-oxide nanotubes could be synthesized by the immersion of carbon nanofiber templates into metal nitrate solutions and removal of the templates by heat treatment in air.

Nickel–aluminum layered double hydroxides prepared via inverse micelles formation

María E. Pérez-Bernal, Ricardo J. Ruano-Casero, Fátima Benito and Vicente Rives

Page 1593

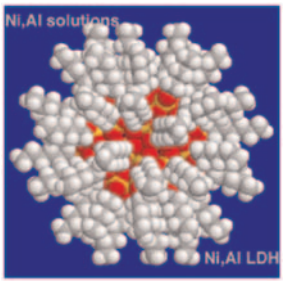

Nickel–aluminum layered double hydroxides have been prepared by conventional coprecipitation and by coprecipitation in the presence of a surfactant. It has been found that both the preparation method and the calcination treatment have an important effect on the luminosity (whiteness/darkness) of the solids, although the effect on the precise chromaticity coordinates (green/red and blue/yellow) is less marked.

Author inquiries

For inquiries relating to the submission of articles (including electronic submission where available) please visit this journal's homepage at http://www.elsevier.com/locate/jssc. You can track accepted articles at http://www.elsevier.com/trackarticle and set up e-mail alerts to inform you of when an article's status has changed. Also accessible from here is information on copyright, frequently asked questions and more.
Contact details for questions arising after acceptance of an article, especially those relating to proofs, will be provided by the publisher.

Language services. Authors who require information about language editing and copyediting services pre- and post-submission please visit http://www.elsevier.com/locate/languagepolishing or our customer support site at http://epsupport.elsevier.com. Please note Elsevier neither endorses nor takes responsibility for any products, goods or services offered by outside vendors through our services or in any advertising. For more information please refer to our Terms & Conditions http://www.elsevier.com/termsandconditions

For a full and complete Guide for Authors, please go to: http://www.elsevier.com/locate/jssc

Journal of Solid State Chemistry has no page charges.